JOURNAL
of the AMERICAN CERAMIC SOCIETY
Volume 60, Number 1-2 January-February, 1977

A One-Dimensional Model of Stretching Float Glass

O. S. NARAYANASWAMY*
Engineering and Research Staff, Ford Motor Company, Dearborn, Michigan 48121

One of the important steps in the manufacture of glass by the float process is the control of glass thickness by stretching the ribbon. The first step in a program to model the stretching of float glass is discussed. A simple, 1-dimensional analysis is presented for the mechanics of stretching a free ribbon, i.e. one without edge constraints in the stretching region. For the case of a stiff ("cold") ribbon, the present analysis yields closed-form solutions which are generally valid but do not encompass all phenomena of interest. The stretching of a "hot" ribbon is, therefore, treated quantitatively by computer simulation. This approach is used to illustrate the differential attenuation of the width and thickness of hot ribbons. In another numerical example, the calculated width attenuation is compared with the results of in-plant measurements.

I. Introduction

When the invention of the float glass process was first announced, only glass ≈0.27 in. thick could be made; eventually 0.27-in. float glass was stretched to yield thinner glass. Since then, the float process has largely replaced the older plate glass process for manufacturing flat glass. Pilkington[1] has given an excellent account of how the process was developed, the different problems encountered, and their solution through experimentation and analysis.

The float glass process exploits the fact that molten glass poured on molten tin spreads out to a perfectly flat sheet. This glass sheet has an equilibrium thickness of ≈0.27 in., determined by the surface tensions of glass, tin, and the glass-tin interface and by the densities of glass and tin (see Fig. 1). The surface tension forces that help form glass of equilibrium thickness also work against forming thinner glass. An analysis of the factors governing the equilibrium thickness showed that there is little scope for changing these factors to obtain a significant reduction in thickness. However, a substantial reduction in thickness can be obtained by the mechanical stretching of glass ribbon. The physical phenomena involved are discussed in the papers of Pilkington[1] and Charnock.[2]

To treat the subject quantitatively, the present paper proposes a 1-dimensional model of stretching which describes the process in the simplest possible terms without losing sight of the essentials. Thus, it is a prelude to a 2-dimensional finite-element model of stretching which also accounts for 2-dimensional variations in temperature, velocity, thickness, and stress in the ribbon.

II. Description of Ribbon Stretching

A float glass ribbon can be stretched successfully when a certain viscosity regime, i.e. a longitudinal temperature distribution in the tin bath, is followed. Figure 2(*A*), taken from Pilkington's paper,[1] shows the appropriate viscosities for 4 stages of the process. Figure 2(*B*) indicates the corresponding temperature distribution.

In the first stage of the process, molten glass is poured onto molten tin and allowed to spread out to its equilibrium thickness. The temperature in this region, ≈1950°F, is high enough to allow any surface irregularities to even out by flow (viscosity = 10^4 P) and to ensure uniform thickness. Second, the glass is cooled to 1300°F (≈10^8 P) and the ribbon edges are gripped by pairs of edge rollers.

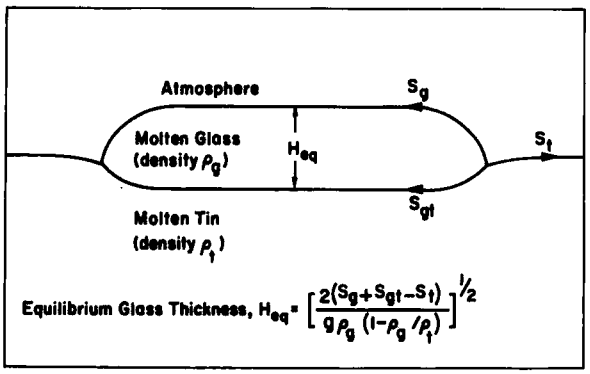

Fig. 1. Equilibrium thickness of molten glass floated on molten tin.

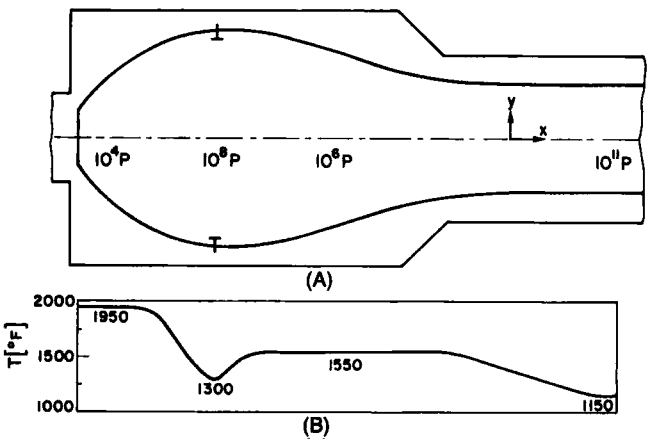

Fig. 2. (*A*) Viscosity and (*B*) temperature regime for stretching float glass ribbon.

Received June 11, 1976.
*Member, the American Ceramic Society.

The speed of the rollers determines the local speed and width of the ribbon. These rollers also counteract the longitudinal tractive force applied to stretch the ribbon and thus prevent the transmission of this large force to the low-viscosity glass upstream. In the third stage, the ribbon is reheated to ≈1550°F. The corresponding viscosity of $\approx 10^6$ P is low enough to allow stretching without the generation of excessive stresses, and yet high enough to prevent surface tension forces from driving the thickness back to its equilibrium value. Finally, in the fourth stage, the ribbon is cooled to 1100°F ($\approx 10^{11}$ P). Now the ribbon is hard and stiff enough to be removed mechanically from the tin bath without surface damage. The temperature distribution shown in Fig. 2(*B*) represents an ideal situation. Large departures from the suggested temperatures can bring about an altogether different balance of forces that, in turn, can lead to failure of the stretching process.

III. Analysis of Ribbon Stretching

The present analyses idealize ribbon stretching as a largely 1-dimensional flow in the presence of a 1-dimensional (longitudinal) temperature distribution. The assumptions of this idealization are described by:

$$\sigma_x=\sigma_x(x), \quad \sigma_y=\sigma_y(x), \quad \sigma_z\equiv 0 \tag{1a}$$

$$\dot{u}_x=\dot{u}_x(x), \quad \dot{u}_y=[f(x)]y, \quad \dot{u}_z=[g(x)]z \tag{1b}$$

$$W=W(x), \quad H=H(x) \tag{1c}$$

$$T=T(x) \tag{1d}$$

In Eq. (1), σ represents stress components, $\dot{u}$ velocity components, W and H the width and thickness of the ribbon, and T the ribbon temperature. The simplifications just given result from the low ratios of the ribbon width and thickness to its length. In a 2-dimensional analysis, all of the variables except W are allowed to vary along both the axial (x) and transverse (y) directions. Computer runs based on the 2-dimensional model have confirmed the validity of the assumptions in Eqs. (1*a*), (1*b*), and (1*c*) for ribbons with a 1-dimensional temperature distribution.

(1) Stiff-Ribbon Analysis

At the stretching temperature (≈1550°F), the ribbon is stiff and viscous forces are dominant. Forces such as surface tension, inertia, and hydrostatic pressure are negligible. The drag of the molten tin on the moving ribbon may be important, depending on the nature of convection currents in the tin. However, this effect is ignored in the present 1-dimensional model, which aims to predict only the gross dimensions of the ribbon. In addition, when there are no edge rollers in the stretching region ("free ribbon"), the transverse stress (σ_y) is zero. Under these conditions, the axial tractive force does not vary along the length of the ribbon, i.e.

$$F=WH\sigma_x=\text{constant} \tag{2}$$

The axial stress and velocity gradient are related by:

$$\sigma_x=\frac{F}{WH}=3\eta\frac{d\dot{u}}{dx} \tag{3}$$

where η is the viscosity of glass. At steady state, the mass flow at any cross section is a constant. Therefore,

$$\rho WH\dot{u}=\dot{m}=\text{constant} \tag{4}$$

Eliminating W and H in Eqs. (3) and (4) gives

$$\frac{F\rho\dot{u}}{\dot{m}}=3\eta\frac{d\dot{u}}{dx} \tag{5}$$

The solution of differential Eq. (5) is

$$\ln\frac{\dot{u}}{\dot{u}_1}=\frac{F\rho}{\dot{m}}\int_0^x\frac{dx}{3\eta(x)}=\frac{[\ln(\dot{u}_n/\dot{u}_1)](x/x_n)}{(\bar{\eta}/\bar{\eta}_n)} \tag{6a}$$

or

$$\dot{u}(x)=\dot{u}_1\exp[S(x)] \tag{6b}$$

In Eq. (6) and the following, subscript 1 stands for the initial value at the edge rolls and subscript n for the final (downstream) value.

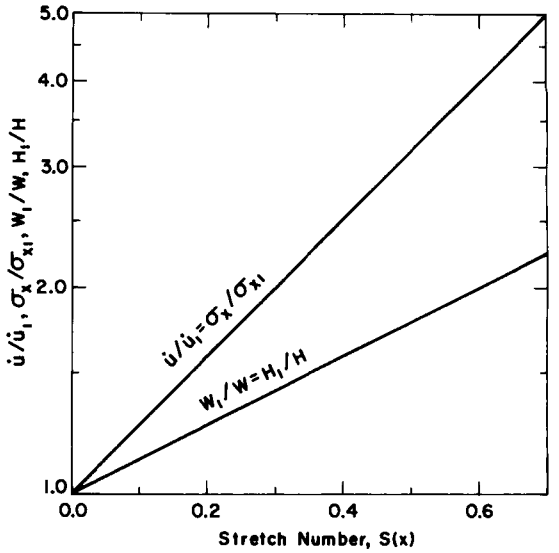

Fig. 3. Solutions of stiff-ribbon analysis.

Equation (6) leads to the following definitions of a nondimensional local stretch number, $S(x)$ and local effective viscosity, $\bar{\eta}(x)$:

$$S(x)=(x/x_n)(\bar{\eta}_n/\bar{\eta})\ln(\dot{u}_n/\dot{u}_1) \tag{7}$$

$$\frac{1}{\bar{\eta}(x)}=\frac{1}{x}\int_0^x\frac{dx}{\eta(x)} \tag{8}$$

From the mass-conservation equation, it follows that $WH\dot{u}=W_1H_1\dot{u}_1$ or $(W/W_1)(H/H_1)=\dot{u}_1/\dot{u}$. Since glass is isotropic and $\sigma_y=0$ (because surface tension is neglected), the width and thickness of the ribbon are attenuated in the same proportion. Thus, $(W/W_1)(H/H_1)=(W/W_1)^2=(H/H_1)^2=\dot{u}_1/\dot{u}$ or

$$W(x)=W_1\exp[-\tfrac{1}{2}S(x)] \tag{9a}$$

$$H(x)=H_1\exp[-\tfrac{1}{2}S(x)] \tag{9b}$$

The axial stress is derived from Eqs. (3) and (6).

$$\sigma_x=3\eta\frac{d\dot{u}}{dx}=3\dot{u}\left(\frac{\bar{\eta}_n}{x_n}\right)\ln\frac{\dot{u}_n}{\dot{u}_1} \tag{10a}$$

or

$$\frac{\sigma_x}{\sigma_{x_1}}=\frac{\dot{u}}{\dot{u}_1}=\exp[S(x)] \tag{10b}$$

Equations (6), (9), and (10) completely describe the stretching process and are used to calculate velocity, width (or thickness), and stress at any cross section along the length of the ribbon. These equations clearly indicate that the plots of $\log \dot{u}/\dot{u}_1$, $\log W_1/W$, $\log H_1/H$, and $\log \sigma_x/\sigma_{x_1}$ are all linear functions of the nondimensional number S as shown in Fig. 3. The S number describes what fraction of the total stretching has occurred up to a given point; S may, therefore, also be regarded as a dimensionless measure of position along the float bath: It increases from zero at the upstream end ($x=0$) to a maximum of $\log \dot{u}_n/\dot{u}_1$ at the downstream end ($x=x_n=L$). Thus, a relation between S_{max} and the stretch ratio, R, is obtained from Eq. (7):

$$R=\dot{u}_n/\dot{u}_1=\exp[S_{max}] \tag{11}$$

The importance of the concepts of effective viscosity $\bar{\eta}$ and stretch number S is that they permit simple and universal solutions for the entire family of stiff-ribbon problems. These solutions (Eqs. (6), (9), and (10)) are independent of mass flow, stretch ratio, temperature distribution, etc. for any given design of the ribbon stretching operation.

(2) Comprehensive 1-Dimensional Analysis

The stiff-ribbon analysis neglects the surface tension forces and, hence, fails to predict differential attenuation in a hot ribbon. A

more comprehensive, yet 1-dimensional analysis of stretching that accounts for all forces acting on the ribbon (viscous, surface tension, inertia, and hydrostatic pressure) is free of this limitation. The exact (comprehensive) analysis was also used to validate the results of the approximate (stiff-ribbon) analysis. Furthermore, the experience gained in the numerical solution of the exact equations of 1-dimensional flow proved useful in the numerical solution of the more complex 2-dimensional flow problem.

In the comprehensive analysis, the steady-state shape of the stretched ribbon is not known in advance. It may be calculated by making an initial guess of the shape and performing a series of iterations until convergence is obtained. Alternatively, one can start with a known solution and calculate transients leading to the desired solution. The latter approach, although time-consuming, is sure-footed. Therefore, the computer simulation starts with a rectangular ribbon of constant width (W_1) and thickness ($H_1 = H_{eq}$), moving with uniform axial velocity ($\dot{u}_1$). The downstream velocity is then increased to $\dot{u}_n$ and a transient solution is calculated every $\Delta t (\simeq 5)$ s. A steady state is reached when the ribbon shape remains unchanged for 2 consecutive time steps.

The axial momentum balance at any cross section of the ribbon is written in Eulerian framework as follows:

$$\frac{\partial F}{\partial x} - \frac{\partial W}{\partial x} H\sigma_y - 0.5\rho g \frac{\partial (WH^2)}{\partial x} - (\rho WH)\frac{D\dot{u}}{Dt} = 0 \qquad (12)$$

where $D/Dt = \partial/\partial t + \dot{u}(\partial/\partial x)$ is the total derivative. The 4 terms of Eq. (12) represent contributions from axial traction (viscous), surface tension, hydrostatic pressure, and inertia. The velocity gradient is related to stress components by

$$\frac{\partial \dot{u}}{\partial x} = \frac{1}{3\eta}(\sigma_x - 0.5\sigma_y) = \frac{F}{3\eta WH} - \frac{0.5\sigma_y}{3\eta} \qquad (13)$$

In Eq. (13), Poisson's ratio is taken to be 0.5, since glass is practically incompressible.

The transverse stress σ_y is the result of surface tensions and hydrostatic pressures acting at the edge of the ribbon; $\sigma_y = 0$ wherever $H = H_{eq}$. The exact expression for this stress component (see Ref. 3) is

$$\sigma_y = \tfrac{1}{2} g \rho_g H_{eq}^2 \left(1 - \frac{\rho_g}{\rho_t}\right)\left(\frac{H^2}{H_{eq}^2} - 1\right) \qquad (14)$$

When $H > H_{eq}$, σ_y is tensile and the ribbon tends to expand; when $H < H_{eq}$, σ_y is compressive and the ribbon tends to contract. Accordingly, W varies with time. This variation is governed by

$$\frac{\partial W}{\partial t} = W\dot{\varepsilon}_y - \dot{u}\frac{\partial W}{\partial x} \qquad (15a)$$

Similarly, the variation in thickness is given by

$$\frac{\partial H}{\partial t} = H\dot{\varepsilon}_z - \dot{u}\frac{\partial H}{\partial x} \qquad (15b)$$

In Eq. (15), the first term on the right side represents actual deformation of the material and the second term reflects dimensional changes resulting from the axial movement of the ribbon. At steady state, these 2 effects cancel out and an unchanging ribbon shape results.

Equations (12), (13), and (15), which represent momentum balance, constitutive relation, and mass balance, respectively, are generalizations of Eqs. (2), (3), and (4) of the stiff-ribbon analysis. Unlike the latter, the equations of the comprehensive analysis are too complex to admit closed-form solutions and were solved numerically. Details of the numerical formulation will not be given here, except to mention that the numerical method of solution is stable only when the calculation proceeds in the downstream direction.

IV. Results

Before discussing results as such, it is useful to illustrate the operation of the present computer simulation of the drawing of a float-glass ribbon. Figure 4 shows a sequence of transient ribbon configurations obtained during the generation of a steady-state solution for the ribbon pulled at 1550°F (see Fig. 5). The simulation

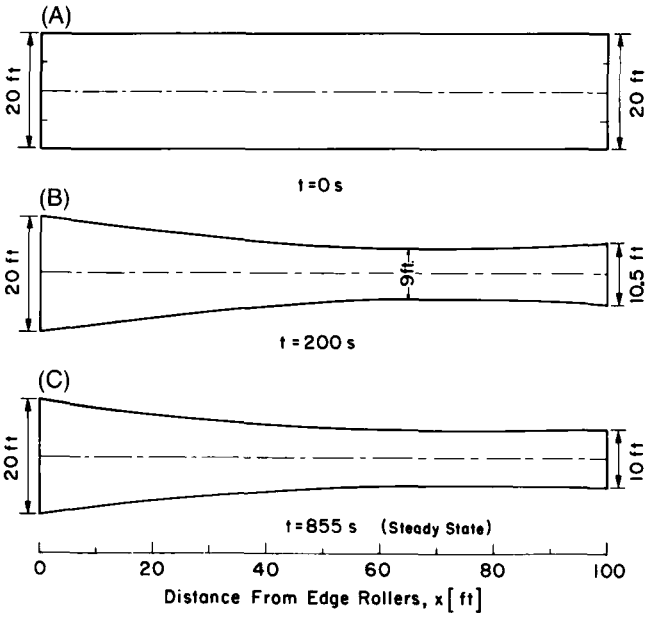

Fig. 4. Transient ribbon shapes.

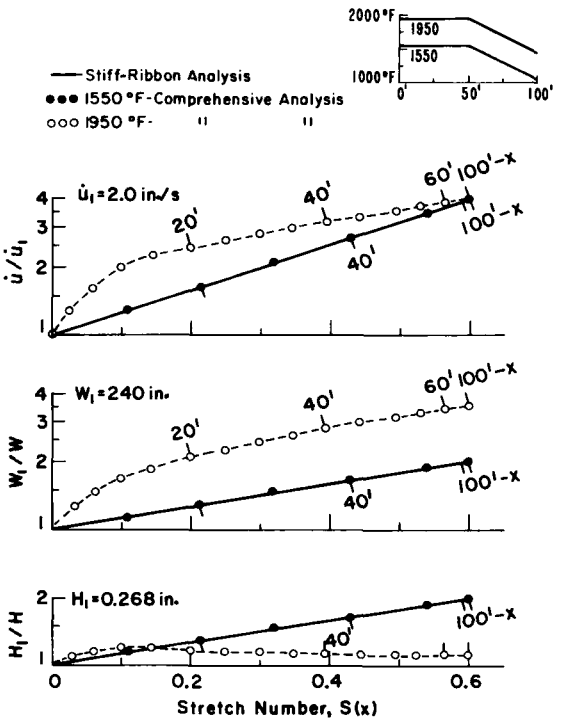

Fig. 5. Steady-state solutions for "hot" (1950°F) and "cold" (1550°F) ribbons.

starts with a known solution, i.e. a ribbon of equilibrium thickness with constant width and axial velocity along its entire length. At $t = 0$, the downstream velocity is increased to 4 times its initial value, causing a greater mass flow at the downstream end than at the upstream end. As a result of this imbalance, a neck develops in the middle of the ribbon (see Fig. 4(*B*)). The neck travels downstream and finally a ribbon with monotonically decreasing width is obtained; this steady-state shape results after 855 s of simulated pulling. At this time, the mass flow across any cross section of the ribbon is constant to within 0.1%. The steady-state shape indicates that >90% of the stretching occurs in the first 50 feet in which the

temperature is held constant at 1550°F. Very little stretching occurs as the ribbon is pulled 50 feet farther and cooled linearly to 1050°F. All further results will refer to ribbons in the steady state of stretching.

Four numerical examples are presented in the following sections. The first 2 are chosen to contrast the stretching characteristics of "cold" and "hot" glass ribbons. The third examines differential attenuation of glass ribbon as a function of its temperature. The fourth compares the calculated width attenuation with measurements obtained from a typical plant run.

(1) Comparison of Stretching "Cold" and "Hot" Ribbons

For the examples given in this section, the following operating conditions are assumed: mass flow, $\dot{m} = 500$ tons/day; upstream width, $W_1 = 240$ in.; upstream thickness, $H_1 = 0.268$ in.; and stretch ratio, $\dot{u}_n/\dot{u}_1 = 4$. The ribbon is assumed to be held at a constant high temperature for the first 50 feet of stretching, and it is cooled linearly in the next 50 feet to freeze in its shape. Thus, the ribbon is stretched at essentially constant temperature. As Fig. 5 shows, 2 cases are considered: In one the glass is stretched at 1550°F, in the other at 1950°F. Calculations are performed both by the simpler stiff-ribbon analysis and the comprehensive analysis. Meaningful calculations for the hot ribbon require use of the comprehensive analysis. The results are given in Fig. 5, which shows the local velocity, width, and thickness (all plotted in a nondimensional form) as functions of the local stretch number, $S(x)$. An x scale denoting physical distance from the edge rollers is marked along each curve. Note, at the downstream end, the crowding of this scale, which reflects the freezing in of the ribbon shape. Finally, Fig. 6 shows the axial stress as a function of x. In these graphs, solid lines represent results of the stiff-ribbon analysis, and plotted points the results obtained by the comprehensive analysis.

The cold ribbon example uses a stretching temperature of 1550°F, as suggested in Ref. 1. As shown by Figs. 5 and 6, the same steady-state distributions of axial velocity, width, thickness, and axial stress are obtained by both the stiff-ribbon and the comprehensive analyses. This agreement shows that, for the stretching of sufficiently cold ribbons, the simpler stiff-ribbon analysis yields very good results.

In a hot ribbon, surface irregularities are rapidly removed by viscous flow. Thus it might appear desirable to stretch glass at high temperatures. However, any attempt to stretch a really hot ribbon produces large differential attenuation, i.e. very little attenuation in thickness and unacceptably high attenuation in width. The second of the present examples, in which a glass ribbon is stretched at 1950°F, is chosen to illustrate differential attenuation at its worst.

The open circles in Figs. 5 and 6 represent the steady-state solutions for the stretching of a hot ribbon as obtained by the comprehensive analysis. These results, unlike those for the cold ribbon (solid circles), differ greatly from the results of the stiff-ribbon analysis (solid lines). The differences are the result of surface tension, inertia, and hydrostatic forces that are included in the comprehensive analysis. The influence of surface tension on the differential attenuation of width and thickness is especially marked at high temperatures, as is shown in the 2 lower plots in Fig. 5. Thus, in response to a 4-fold increase in axial velocity, the thickness attenuation is practically negligible ($H_1/H_n = 1.13$); almost all attenuation occurs in width ($W_1/W_n = 3.53$). Thus, the hot-ribbon example illustrates the kind of problem Pilkington faced in the early stages of developing the float process for thin (<0.268 in.) glass.

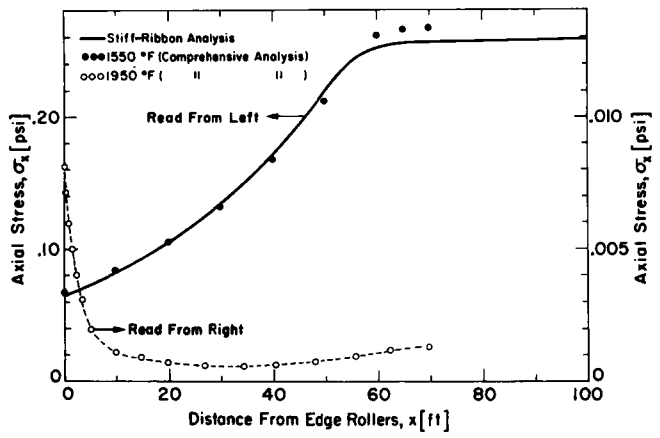

Fig. 6. Axial stresses in "hot" and "cold" ribbons.

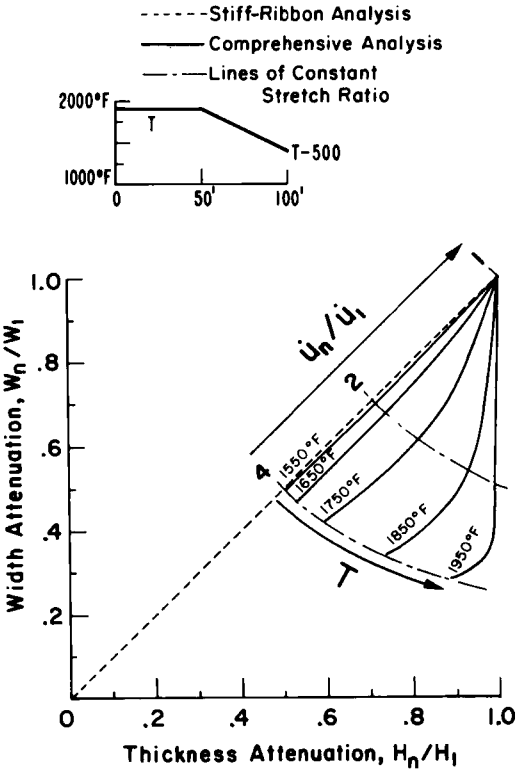

Fig. 7. Ribbon attenuation at different temperature and stretch ratios.

(2) Differential Attenuation and Ribbon Temperature

The examples just given demonstrate that differential attenuation is negligible at 1550°F and quite unacceptably large at 1950°F. This problem is addressed more generally in Fig. 7, a plot of width and thickness attenuation as functions of stretching temperature and stretch ratio, $\dot{u}_n/\dot{u}_1$. Figure 7 illustrates the results of a computer simulation of the stretching process and uses the dimensionless parameters W_n/W_1 and H_n/H_1; thus this figure also generalizes Fig. 16 of Pilkington's paper that was drawn in terms of the physical variables W_n and H_n and based on data from plant trials. It is evident from Fig. 7 that the best temperature for stretching glass ribbon is 1550°F; higher temperatures produce large differential attenuation and lower temperatures induce larger stresses in glass ribbon than are necessary for stretching. The ribbon temperature for stretching may therefore be specified as 1550°F with a tolerance of ±50°F.

(3) Comparison of Model Results and Plant Data

A comparison of the calculated predictions of process parameters with representative data from an actual float glass plant operating with a single pair of edge rollers is illustrated in part by Fig. 8 for the following operating conditions: mass flow, $\dot{m} = 300$ tons/day; ribbon width near edge rollers, $W_1 = 225$ in. (upstream width); edge-roller speed, $\dot{u}_1 = 71.1$ in./min (upstream velocity); and lehr speed, $\dot{u}_n = 400$ in./min (downstream velocity). The axial temperature variation along the length of the ribbon is shown in Fig. 8(*A*). The fact that the ribbon edges are somewhat colder than the center is ignored by the present 1-dimensional model used to simulate the plant run. Stiff-ribbon analysis is used because the ribbon is relatively cold (maximum axial temperature in the stretching re-

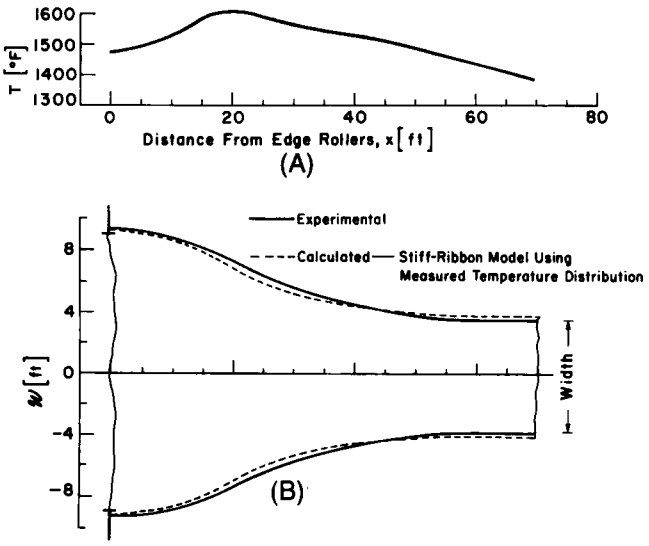

Fig. 8. Ribbon width as a function of position in tin bath.

gion = 1605°F). Fig. 8(*B*) shows the predicted (dotted lines) and measured shapes of the ribbon; there is good agreement between the two. Calculated and measured downstream width and thickness are compared in Table I. The width attenuation in the first 40 feet could be predicted more accurately by estimating the influence of the lateral pull exerted by the edge rollers.

V. Conclusions

The stretching of float glass is largely governed by the viscosity of the ribbon in the stretching region. Differential attenuation of width and thickness can be avoided if the ribbon viscosity is $\approx 10^6$ P ($T \simeq 1550$°F). For such stiff ribbons, simple solutions for flow variables are obtained in terms of a nondimensional stretch number S. The solutions cover the entire class of stiff-ribbon problems. In nondimensional form, they are independent of operating conditions such as mass flow, stretch ratio, and temperature variations along the ribbon.

Differential attenuation is predicted in stretching a hot ribbon, in agreement with Pilkington's observation. It is further shown that a ribbon could be as hot as 1600°F without showing appreciable differential attenuation.

Calculated width attenuation (based on stiff-ribbon analysis) is in good agreement with in-plant measurements. This good agreement also indicates that the final width and thickness are not very sensitive to the moderate temperature variations that existed across the width of the ribbon.

Table I. Calculated and Measured Dimensions of Downstream Ribbon

Data source	Width (in.)	Thickness (in.)
Plant data	91	0.127
Stiff-ribbon analysis	95	.122
Comprehensive analysis	93	.125

Acknowledgments: R. Gardon is thanked for valuable discussions and J. Sowman and E. Augustin for furnishing plant data on stretching.

References

[1] L. A. B. Pilkington, "Float Glass Process," *Proc. R. Soc. London, Ser. A*, **314** [1516] 1–25 (1969).
[2] Harold Charnock, "Float Glass Process," *Phys. Bull.*, **21** [4] 153–56 (1970).
[3] Irving Langmuir, "Oil Lenses on Water and the Nature of Monomolecular Expanded Films," *J. Chem. Phys.*, **1**, 756–76 (1933).

Kernel Migration for HTGR Fuels from the System Th-U-Pu-C-O-N

T. B. LINDEMER* and R. L. PEARSON*

Chemical Technology Division, Oak Ridge National Laboratory, Oak Ridge, Tennessee 37830

Nuclear fuels for the high-temperature gas-cooled reactor (HTGR) consist of spherical kernels of actinide compounds contained in gastight pyrolytic carbon and SiC. The fuel kernels migrate up the temperature gradient and into the coating layers. A theoretical analysis of in-reactor migration data indicates that a solid-state diffusion process controls the migration rate in fissioned $Th_{0.84}U_{0.16}C_2$, UO_2, ThO_2, PuO_{2-x}, and $Th_{0.8}U_{0.2}O_2$ particles. The theoretically based kernel migration coefficient (KMC) measured in units (cm/s) °K² (°K/cm)$^{-1}$, is thus used to correlate the laboratory and in-reactor data. The KMC values for Pu-containing particles may be dependent on the initial and in-reactor O/Pu values. The other in-reactor KMC values were apparently not dependent on the extent of fission, the fission of either ^{233}U or ^{235}U, or the presence of an SiC coating layer. Laboratory KMC values were obtained for unirradiated ThO_2, $UO_{1.65}N_{0.25}$, UC_2, ThC_2, and $Th_{0.84}U_{0.16}C_2$ particles and generally appeared to be consistent with in-reactor data.

I. Introduction

FUEL elements for high-temperature gas-cooled reactors (HTGR's) are made from rigid assemblies (fuel rods or compacts) of coated fuel particles distributed appropriately in graphite holders that contain coolant passages and constitute both moderator and core structure.[1–3] The coated fuel particles are small spherical oxide or carbide kernels that are each coated with successive layers of pyrolytic carbon (BISO particles) and sometimes an intermediate layer of SiC (TRISO particles). The pyrolytic carbon layers absorb damaging fission fragments and retain gaseous fission products and their precursors, whereas the SiC layer improves the retention of metallic fission products and fuels.[4,5] These fuels are currently

Received February 28, 1976; revised copy received August 9, 1976.
Based in part on presentations to the Nuclear Division of the American Ceramic Society, Paper Nos. 20-N-72, 13a-N-73, 62-N-74, 49-N-74, 5-N-75, and 43-N-75.
Supported by the U.S. Energy Research and Development Administration under contract with Union Carbide Corporation.
*Member, the American Ceramic Society.